J Mater Sci: Mater Electron (2022) 33:13939–13946

Thickness-dependent dielectric and ferroelectric properties of $0.7Bi(Fe_{0.98}Mn_{0.02})O_3$-$0.3PbTiO_3$ thin films on stainless steel substrates

Wenhui Lu[1], Jie Jian[1], Jianguo Chen[1], and Jinrong Cheng[1,*]

[1] *School of Materials Science and Engineering, Shanghai University, 99 Shangda Road, Shanghai 200444, People's Republic of China*

Received: 24 January 2022
Accepted: 23 April 2022
Published online:
17 May 2022

© The Author(s), under exclusive licence to Springer Science+Business Media, LLC, part of Springer Nature 2022

ABSTRACT

In this paper, ferroelectric films of $0.7Bi(Fe_{0.98}Mn_{0.02})O_3$-$0.3PbTiO_3$ (BFM-PT) on $LaNiO_3$ (LNO)-coated stainless steel (SS) substrates with different thicknesses were fabricated by sol–gel process. X-Ray diffraction (XRD) patterns and Scanning electron microscopy (SEM) images reveal that such BFM-PT thin films show single perovskite structure and smooth surface without detected second phase. With the increase of film thickness, BFM-PT thin films exhibit increased maximum polarization (P_{max}) and dielectric constant (ε_r), as well as reduced dielectric loss ($tan\delta$) and leakage current density. The values of remanent polarization (P_r), ε_r and $tan\delta$ (@ 10^3 Hz) for BFM-PT thin films with thickness of 1.2 μm are 21.2 μC/cm^2, 618 and 0.05, respectively. The conduction mechanism of the BFM-PT thin films at low electric field changes from space charge limited conduction (SCLC) to Ohmic conduction with the increase of film thickness. Our results indicate that BFM-PT thin films coated on SS substrates with LNO buffer layer maintain excellent dielectric and ferroelectric properties.

1 Introduction

In recent years, solid solutions of bismuth ferrite ($BiFeO_3$, BF) with other ABO_3 perovskite structure oxides have been received extensive attention from the researchers as alternative to traditional $Pb(Zr_xTi_{1-x})O_3$ (PLZT) piezoelectric materials because of its strong ferroelectric, multiferroic and lead-reduced environmental friendly properties [1–3]. Modified $BiFeO_3$-$xPbTiO_3$ (BF-PT, $x \approx 0.7$) solid solutions ceramics near the morphotropic phase boundary (MPB) obtained the enhanced piezoelectric properties that attribute to the existence of tetragonal and rhombohedral phases [4–7]. It is of great interest to prepare thin film type BF-PT-based solid solutions with comparable dielectric and ferroelectric properties with bulk materials, which are more suitable for applications in microelectro-mechanical systems [8, 9]. In the past few decades, element doping and buffer layer have become efficient and easily available strategies for researchers for the purpose of further improving the performances of BF-PT thin

Address correspondence to E-mail: jrcheng@staff.shu.edu.cn

https://doi.org/10.1007/s10854-022-08324-4

films [6, 7, 10–12]. The sol–gel derived La/Mn co-doped 0.7BF-0.3PT thin films prepared on Si substrates have excellent ferroelectric responses with Mn^{2+} and La^{3+} substitutions for part of Fe^{3+} and Bi^{3+} ions, respectively [10]. Multilayer BF/PT thin films coated on Si substrates been reported the improved ferroelectricity with large value of $P_r \sim 41$ μC/cm^2, which attribute to little variation valence of metal ions in PT layers [11]. BF-*x*PT thin films with low leakage current density have been fabricated by introducing PT buffer layer which forms a Schottky barrier between the substrates and films [12].

In order to meet the application of wearable and flexible electronic devices, ferroelectric thin films are also expected to be deposited on substrates which made by flexible metal foils [13, 14]. The performances of ferroelectric thin films on flexible metal substrates are deeply affected by thermal diffusion of metal elements and lattice mismatch, which can be weakened by the buffer layer with perovskite structure, such as LNO and $LaSrCoO_3$ [15, 16]. These oxide buffer layers not only have more similar lattice parameters of ferroelectric thin films, but also helps to reduce thermal expansion bring by metal substrates [17–19]. By integrating La-doped $PbZrO_3$ (PLZO) thin films on austenitic metal foil substrate with the LNO buffer layer, the comparable energy storage density of PLZO thin films is obtained to that of PLZO thin films on Pt/Si substrate [17]. In our previous work, the dielectric and ferroelectric properties of BST, PLZT and BF-PT thin films on SS substrates have been well explored [15, 16, 18–20]. However, the influence of metal substrates on the growth process of BF-PT thin films and the thickness-dependent properties are rarely reported.

In this work, $0.7Bi(Fe_{0.98}Mn_{0.02})O_3$-$0.3PbTiO_3$ (BFM-PT) thin films with different thicknesses were fabricated on the stainless steel (SS) substrates with incorporation of the $LaNiO_3$ buffer layer by the sol–gel technique. The dielectric and ferroelectric properties of BFM-PT thin films were studied as a function of film thickness, the conduction mechanism of BFM-PT thin films was also investigated.

2 Experimental procedures

$0.7Bi(Fe_{0.98}Mn_{0.02})O_3$-$0.3PbTiO_3$ thin films with thickness of 0.3, 0.6, 0.9 and 1.2 μm were synthesized on SS by the sol–gel progress. $Bi(NO_3)_3{\cdot}5H_2O$, $Fe(NO_3)_3{\cdot}9H_2O$, $Pb(CH_3COO)_2$, $Ti(OC_4H_9)_4$ and $Mn(CH_3COO)_2{\cdot}4H_2O$ were mixed according to the stoichiometric ratio in 2-methoxyethanol, then the mixture was heated at 90 °C and stirred at 120 rpm for 2 h to obtain 0.4 mol/L BFM-PT precursor. The excess Bi and Pb of 2 at% and 10 at%, respectively, were added to compensate the loss of Bi and Pb during heat treatment. The nitrates of Ni and La were dissolved into acetic acid in the ratio of 1:1 and heated at 90 °C for 2 h to prepare $LaNiO_3$ sol of 0.1 mol/L. LNO sol was spin coated on stainless steel substrate at 3000 rpm at room temperature and annealed at 550 °C for 4 min in O_2 atmosphere to obtain a layer of LNO. The LNO buffer layer reached thickness of around 100 nm by repeating the above steps and heat treated at 700 °C for 10 min in O_2 atmosphere. Finally, BFM-PT solution was spun on the LNO buffer layer and Pt/Si at 3500 rpm at room temperature, and dried at 200 °C for 2 min. Each layer of BFM-PT thin films with thickness of about 70 nm was heated at 300 °C for 2 min and annealed at 580 °C for 3 min rapidly. The procedures were repeated several times to obtain BFM-PT thin films with desired thickness and then annealed at 600 °C for 30 min.

The phase structure of BFM-PT thin films was analyzed by X-ray diffraction (XRD) system (Rigaku D/Max-2200 V, Japan). The surface and cross-sectional morphology of the films were tested using the scanning electron microscopy (FESEM, JEOL, JSM-7000F). The dielectric, ferroelectric and electrical characteristics of BFM-PT thin films were tested by Aglient 4294A Impedance Analyzer and Ferroelectric tester (Precision Premier II).

3 Results and discussion

3.1 Phase structure and surface morphology

XRD results of BFM-PT thin films for different thicknesses on SS substrates are presented in Fig. 1. BFM-PT thin films show pure perovskite structure without detected secondary phases. The intensity of (100) and (110) diffraction peaks become stronger with the increase of BFM-PT thin films thickness, which indicates that the crystallinity of BFM-PT thin films has been well promoted [21]. The crystallinity of BFM-PT thin films is dependent on the thickness of

BFM-PT thin film. The lattice parameters of SS and BF-PT are 2.66 and 4.25 Å, and the thermal expansion coefficient (TEC) of SS substrates and BF-PT are about 18.4×10^{-6} and -4.7×10^{-6}/°C, respectively. Thus, a significant lattice and thermal mismatch have been introduced between SS substrates and BFM-PT thin films, which will produce compressive stress in the BFM-PT thin films, resulting in lattice distortion [15, 22]. Although the introduction of the LNO buffer layer reduces the compressive stress caused by the SS substrates in BFM-PT thin films, the effects of compressive stress still exist. When the thickness of BFM-PT thin film increases, the influences caused by lattice and thermal mismatch will be weakened, which is contribute to the growth of BFM-PT thin films in (100) and (110) planes.

Figure 2a–d show SEM images of BFM-PT thin films on SS substrates for different thicknesses. It is observed that BFM-PT thin films have smooth and compact microstructure, with the average grain size of 20–50 nm approximately. At the same time, the grain size increases with the increase of BFM-PT thin films thickness. The cross-sectional images shown in Fig. 2a′–d′) taken from the fractured surface of BFM-PT thin films indicate the films are well densified with thickness of 0.3, 0.6, 0.9 and 1.2 μm, respectively.

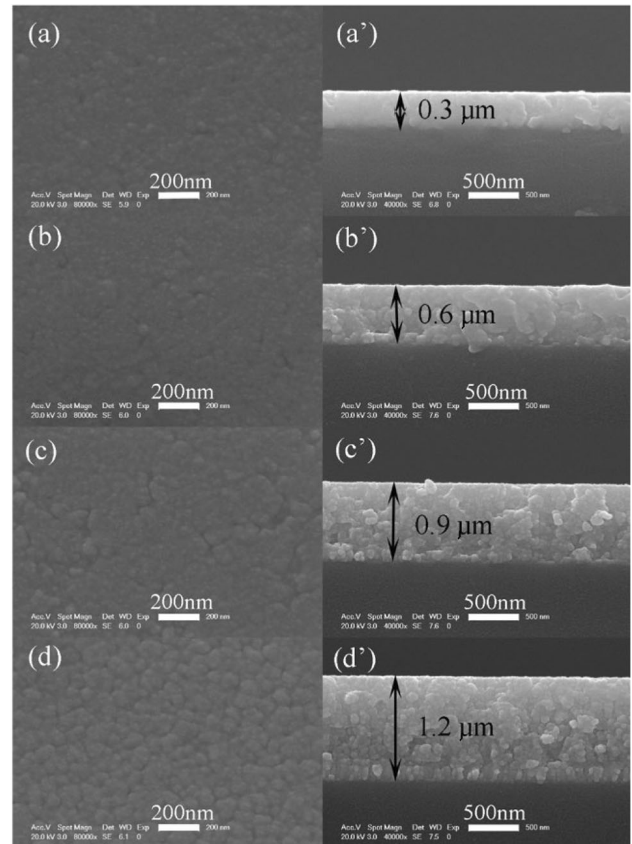

Fig. 2 SEM images of surface and cross-sectional BFM-PT thin films for different thicknesses on SS **a**–**d** and Pt/Si **a'**–**d'** substrates

3.2 Dielectric and ferroelectric properties

The dielectric properties of BFM-PT thin films for different thicknesses are presented in Fig. 3a and b. The dielectric constant (ε_r) of BFM-PT thin films increases gradually with the increase of film thickness, and this trend slows down when the BFM-PT thin film thickness reaches to 0.9 μm. The value of ε_r of BFM-PT thin films increases from 245 to 618 (@ 10^3 Hz), which increases nearly three times, when the thickness of the film is increased from 0.3 to 1.2 μm. Besides, the dielectric constant and loss of BFM-PT thin films with thickness of 0.9 and 1.2 μm display excellent frequency stability. When the film thickness is less than 0.6 μm, BFM-PT thin films have large dielectric loss which dramatically increases with the increase of frequency.

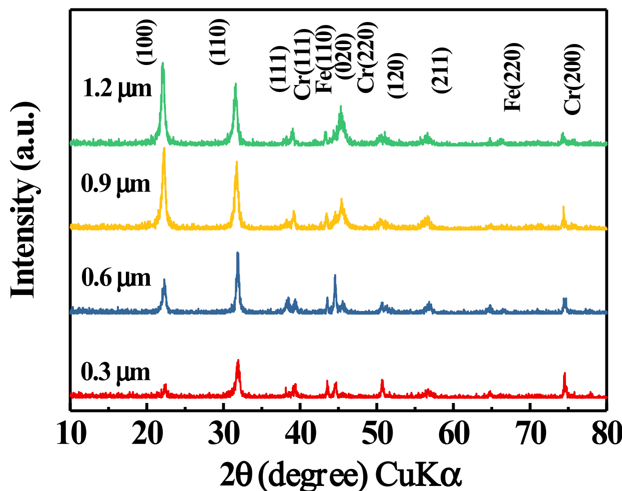

Fig. 1 XRD patterns of BFM-PT thin films for different thicknesses on SS substrates

It is reported that the relationships between film thickness and dielectric properties of ferroelectric thin films are closely related to the dead layer with low permittivity between substrates and ferroelectric thin films [23, 24]. Because of metal element diffusion and lattice mismatch, the dead layer often with thickness of several nanometers appears at the interface between electrode and substrate and films. For parallel plate capacitor structure, the relationship

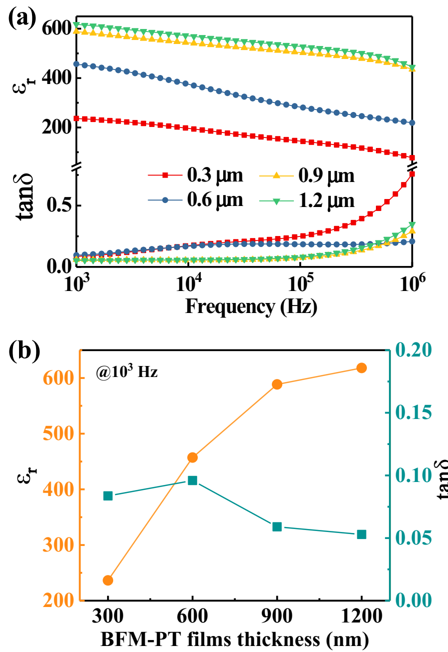

Fig. 3 Dielectric properties of BFM-PT thin films for different thicknesses on SS substrates

between the ε_r of BFM-PT thin films and low permittivity interface layer can be explained by the low permittivity model. The interface layer influences the ε_r with the BFM-PT thin film thickness d, which is described as

$$\frac{d}{\varepsilon_r} = \frac{d_i}{\varepsilon_i} + \frac{d_s}{\varepsilon_s} + \frac{d_f}{\varepsilon_f}(d_f >> d_s, d_f) \quad (1)$$

where ε_i, ε_s and ε_f are the permittivity of interface layer on the bottom and top electrode and the permittivity of the BFM-PT thin films, respectively; d_i, d_s and d_f are the thickness of the interface layer on the bottom and top and the films. The thicker the dead layer, the smaller the dielectric constant of the film. Meanwhile, with the increasing thickness of BFM-PT thin films, the influence of dead layer on dielectric properties decreases gradually and the dead layer is no longer the main factor affecting the dielectric properties of films [23–25]. The compressive stress caused by the substrate lattice mismatch and thermal expansion also significantly affect the values of ε_r and $tan\delta$ of BFM-PT thin films. As the thickness of BFM-PT thin films increases, the compressive stress is gradually released [15, 16, 18]. Besides, BFM-PT thin films with thickness of 0.9 and 1.2 μm have large grain size, which indicates that the volume fraction of grain boundary reduces, so that the restriction of grain boundary is reduced on domain switching during polar process [26, 27]. As the consequence, the value of ε_r for BFM-PT thin films increases and $tan\delta$ decreases as the increasing grain size and film thickness.

Figure 4a presents the *P-E* loops of BFM-PT thin films for different thicknesses at room temperature. When the BFM-PT thin films thickness is greater than 0.3 μm, all samples have saturated slender loops. Figure 4b shows thickness-dependent maximum polarization (P_{max}) and coercive field (E_c) of BFM-PT thin films. When the film thickness is increasing, the saturation polarization of BFM-PT thin films increases gradually and E_c decreases, while the P_r changes slightly. When the thickness of BFM-PT thin films increases from 0.3 to 1.2 μm, the value of E_c decreases from 305 to 108 kV/cm, which decreased by nearly 64%, and the value of P_{max} for BFM-PT thin films enlarges from 30.6 to 43.7 μC/cm^2, which increased by 42.8%.

When the thickness of BFM-PT thin films is low, the compressive stress introduced by lattice and thermal mismatch will form a clamping effect in thin films, which will make the dipole switch more difficultly [15, 28]. Thus, BFM-PT thin films with

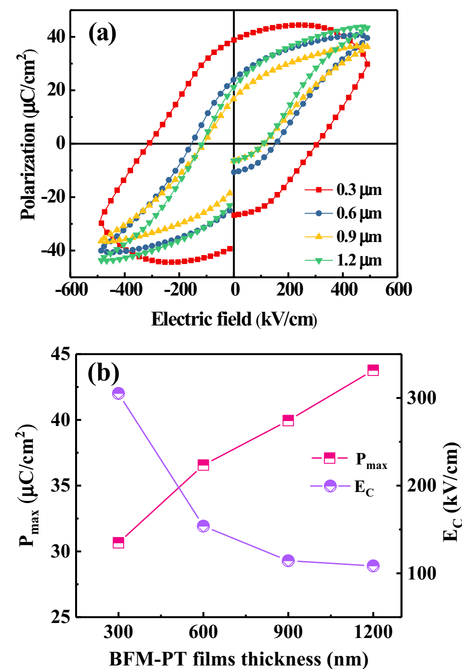

Fig. 4 a Hysteresis loop and **b** maximum polarization and coercive field of BFM-PT thin films for different thicknesses on SS substrates

thickness of 0.3 μm have large coercive field. As for the improving polarization of BFM-PT thin films, on the one hand, the influences caused by dead layer decrease with the increase of thickness. On the other hand, the increase of film thickness leads to increasing grain size, which makes the volume of grain boundary decrease, so that greater polarization can be obtained for BFM-PT thin films [29–31]. The important electrical properties of BFM-PT thin films are collected in Table 1.

3.3 Analysis of leakage current mechanism

The *J-E* characteristics of BFM-PT thin films for different thicknesses on SS substrates are presented in Fig. 5. BFM-PT thin films with thickness of 0.3 μm have the highest leakage current density, which reaches nearly 0.1 A/cm^2 at 250 kV/cm. When the thickness of BFM-PT thin films increases to 1.2 μm, leakage current density decreases by two orders of magnitude compared with that of 0.3 μm, which also corresponds to its sharp and saturated hysteresis loops. The essential factors affect leakage current in BFM-PT thin films are the transport oxygen vacancies generated by lack of Bi and fluctuating valence states of Fe iron (Fe^{3+}/Fe^{2+}). Besides, the interface layers with large amount of charges between the films and the electrode are also important factors of the film conduction mechanism [31, 32]. The *J-E* curves asymmetry of BFM-PT thin films in positive and negative electric field decreases gradually with the increase of film thickness, which indicates that the conduction of the BFM-PT thin film shifts from the interface limitation to the bulk-dominated. This is because the concentration of metal elements diffused into the film decreases with the increase of BFM-PT thin film thickness, which ameliorates the insulation of BFM-PT thin films [33].

In order to further clarify the conductive mechanism of BFM-PT thin films, the *lnJ-lnE* curves are obtained by fitting process as shown in Fig. 6a. It is found that the slope of *lnJ-lnE* for BFM-PT thin films with thicknesses of 1.2 μm is 1.33 and close to "1" at low electric field, which indicate that the Ohmic conduction is the main conduction mechanism [34]. This is due to the effects of dead layer and diffusion concentration of metal elements in BFM-PT thin films are reduced with increasing film thickness. Ohmic conduction can be expressed by the equation

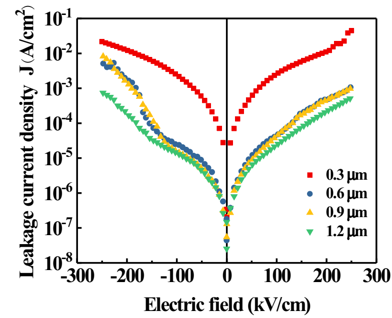

Fig. 5 Leakage current density of the BFM-PT thin films for different thicknesses on SS substrates

$$J = \frac{q\mu n_0 V}{d} \quad (2)$$

where n_0 represents carrier concentration, q is elementary charge, μ is the charge carrier mobility and V is applied voltage.

In the medium electric field, the existence of a large amount of oxygen vacancies and defect complexes in BFM-PT thin films, which will capture electrons or holes emitted from the electrode under low and medium electric fields, and the trapped charges in the films will accumulate to form an internal electric field, which correspond to changing the slops of *lnJ-lnE*. At this time, the SCLC is the dominant conduction mechanism of all BFM-PT thin films, and the SCLC can be expressed by the equation

Table 1 The values of ε_r, $tan\delta$, P_{max} and E_c of BFM-PT thin films for different thicknesses on SS substrates

Thickness of BFM-PT thin films (μm)	ε_r (@10^3 Hz)	$tan\delta$ (@10^3 Hz)	P_{max} (μC/cm^2)	E_c (kV/cm)
0.3	245	0.084	30.6	305
0.6	457	0.096	36.6	154
0.9	588	0.059	39.9	114
1.2	618	0.053	43.7	108

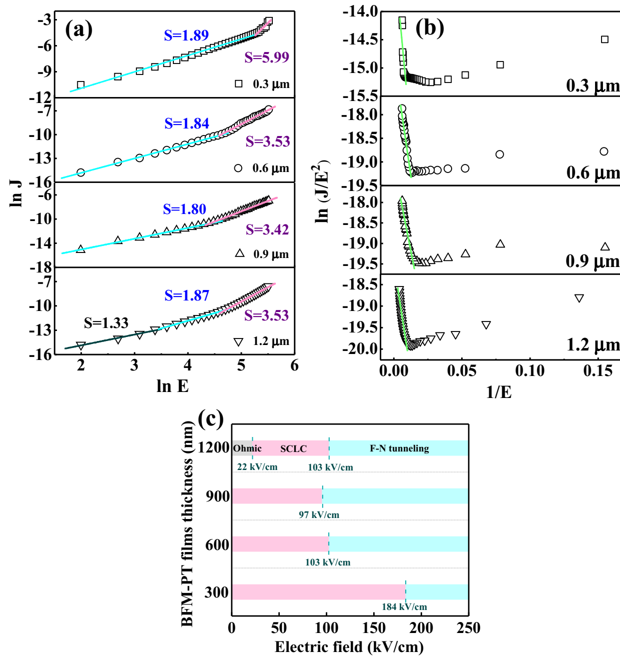

Fig. 6 **a** Ohmic and SCLC conduction mechanism, **b** F-N tunneling process fitting results and **c** an overview of the leakage mechanisms of BFM-PT thin films for different thicknesses on SS substrates

$$J = \frac{9\varepsilon\varepsilon_0\mu V^2}{8d^3} \tag{3}$$

where d is film thickness, ε is the permittivity of ferroelectric film, ε_0 is the vacuum permittivity and V is applied voltage. It is noticed that when the applied electric field is increasing, the slope of *lnJ-lnE* for BFM-PT thin films is greater than "2", and the bulk-limited conduction cannot be explained. [10, 20] Therefore, the $ln\ (J/E^2)\ vs\ 1/E$ function of BFM-PT thin films is presented in Fig. 6b. The linear fitting shows that the main conduction mechanism of all BFM-PT thin films under high electric field is Fowle-Nordheim (F-N) tunneling process, which can be expressed as

$$J_{FN} = AE^2\exp\left(-\frac{B\Phi_i^{3/2}}{E}\right) \tag{4}$$

where Φ_i is the potential barrier height, E is the applied electric field, and A and B are constants. At this time, oxygen vacancies formed by Bi volatilization and carriers accumulate at the interface of the electrode and the films due to the high electric field strength, forming a steeper Schottky barrier which is too thin, so that the current tunnels through the electrode into the BFM-PT thin films [34, 35]. The changes of conduction mechanism with electric field is present in Fig. 6c. It can be seen that the conductive mechanism of the BFM-PT thin films changes from SCLC to F-N tunneling, that is, the process from bulk-dominated to interface limitation. The transition electric fields for this process of BFM-PT thin films with thicknesses of 0.6, 0.9, 1.2 μm are similar, which are greater than that of BFM-PT thin films with thickness of 0.3 μm. This result may be related to the increase of the film surface roughness observed by SEM images (see in Fig. 2). The greater the film roughness, the easier the carrier transport [10, 36].

According to the analysis results of conduction mechanism and *J-E* curves, the conduction mechanism changes when the BFM-PT thin film thicknesses increase to 1.2 μm, and the leakage current density decreases when the film thicknesses greater than 0.3 μm. These results reveal that the change of film thicknesses mainly changes the insulation of BFM-PT thin films and have little effect on the conduction mechanism.

4 Conclusion

BFM-PT thin films for different thicknesses synthesized by sol–gel progress were deposited on stainless steel substrates, and BFM-PT thin films were single perovskite structure and well crystallized. The increasing film thickness is beneficial to obtaining higher values of ε_r and P_{max} of BFM-PT thin films, and reducing the values of $tan\delta$ and E_c. BFM-PT thin films with thickness of 1.2 μm have excellent dielectric and ferroelectric properties. The significant thickness-dependent dielectric properties of BFM-PT thin films resulted from dead layers, lattice and thermal expansion mismatch between BF-PT thin films and SS substrates. The increased thickness of BFM-PT thin films has no obvious influence on the conduction mechanism, however improving the insulation properties of BFM-PT thin films.

Author contributions

WL: contributed to data analysis, writing original manuscript and manuscript modification. JJ: contributed to manuscript modification. JC: helped

perform the analysis with constructive discussions. JC: contributed to the conception of the study, manuscript modification and funding.

Funding

This work was supported by the Open Fund for National Key Laboratory of Science and Technology on Underwater Acoustic Antagonizing (Grant No. JCKY2020207CH02), Original exploration project of Shanghai Natural Science Foundation (Grant No. 22ZR1481100) and National Natural Science Foundation of China (Grant Nos. 51872180 and 51672169).

Data availability

All data generated or analyzed during this study are included in this published article.

Declarations

Conflict of interest We declare that we have no known competing financial interests or personal relationships that could have appeared to influence the work reported in this paper.

Ethical approval The submitted work is original and haven't been published elsewhere in any form or language, and the work will not be submitted elsewhere until the journal editorial procedures are complete.

References

1. J. Wu, Z. Fan, D. Xiao, J. Zhu, J. Wang. Prog. Mater. Sci. **84**, 335 (2016)
2. G. Catalan, J.F. Scott, Adv. Mater. **21**, 2463 (2009)
3. Y. Chu, L.W. Martin, M.B. Holcomb, R. Ramesh, Mater. Today **10**, 16 (2007)
4. W. Zhu, H. Guo, Z. Ye, Phys. Rev. B **78**, 014401 (2008)
5. D.I. Woodward, I.M. Reaney, R.E. Eitel, C.A. Randcall, J. Appl. Phys. **94**, 3313 (2003)
6. H. Amorin, C. Correas, C.M. Fernandez-Posada, O. Pena, A. Castro, M. Alguero, J. Appl. Phys. **155**, 104104 (2014)
7. F. Luo, H. Guan, J. Jian, J. Chen, J. Cheng, J. Am. Ceram. Soc. **102**, 5958 (2019)
8. R. Katoch, R. Gupta, A. Garg, Solid State Commun. **177**, 103 (2014)
9. J.Y. Son, H.W. Shin, J. Alloys Compd. **792**, 673 (2019)
10. D. Chen, J. Cheng, J. Sol-Gel Sci. Technol. **85**, 431 (2018)
11. H. Li, J. Zhu, J. Zhuang, Y. Hu, M. Huai, Q. Yang, J. Sol-Gel Sci. Technol. **75**, 353 (2015)
12. K.K. Sahoo, R. Katoch, K. Brajesh, A. Garg, R. Gupta, J. Appl. Phys. **127**, 064101 (2020)
13. H. Yu, C. Chung, N. Shewmon, S. Ho, J.H. Carpenter, R. Larrabee, L. Sun, J. Jones, H. Ade, B.T. O'Connir, F. So, Adv. Funct. Mater. **27**, 1700461 (2017)
14. J. Rho, S.J. Kim, W. Heo, N. Lee, H. Lee, J. Ahn, IEEE Electron Device Lett. **31**, 1017 (2010)
15. S. Wang, H. Wang, J. Jian, J. Chen, J. Cheng, J. Alloys Compd. **784**, 231 (2019)
16. H. Li, S. Wang, J. Jian, H. Dong, J. Chen, D. Jin, J. Cheng, J. Mater. Sci.: Mater. Electron. **29**, 14651 (2018)
17. H.J. Lee, S.S. Won, K.H. Cho, C.K. Han, N. Mostovych, A.I. Kingon, S. Kim, H.Y. Lee, Appl. Phys. Lett. **112**, 092901 (2018)
18. H. Dong, H. Li, J. Chen, D. Jin, J. Cheng, J. Appl. Phys. **122**, 144104 (2017)
19. H. Dong, G. Lu, D. Jin, J. Chen, J. Cheng, J. Mater. Sci. **51**, 8414 (2016)
20. H. Wang, J. Zhai, W. Lu, J. Chen, J. Cheng, J. Mater. Sci.: Mater. Electron. **32**, 3334 (2021)
21. I. Roh, B. Kwon, S. Baek, S.K. Kim, J. Kim, C. Kang, J. Electron. Mater. **45**, 1057 (2015)
22. S. Song, J. Zhai, L. Gao, X. Yao, S. Lu, Z. Xu, J. Appl. Phys. **106**, 024104 (2009)
23. J. Cheng, L. He, S. Yu, Z. Meng, Appl. Phys. Lett. **88**, 152906 (2006)
24. K. Sekhar, S.H. Key, K.P. Hong, C.S. Han, J.M. Yook, D.S. Kim, J.C. Kim, J.C. Park, Y.S. Cho, Curr. Appl. Phys. **12**, 654 (2012)
25. T. Pecnik, S. Glinsek, B. Kmet, B. Malic, J. Alloys Compd. **646**, 766 (2015)
26. Y. Sudo, M. Hagiwara, S. Fujihara, Ceram. Int. **42**, 8206 (2016)
27. Q. Zhang, Y. Su, J. Appl. Phys. **124**, 144103 (2018)
28. S. Sruthi, A. Adarsh, A. Veronica, M. Saideep, S. Dutta, J. Mater. Sci.: Mater. Electron. **27**, 4062 (2016)
29. M.T. Do, N. Gauquelin, M.D. Nguyen, F. Blom, J. Verbeeck, G. Koster, E.P. Houwman, G. Rijinders, APL Mater. **9**, 021113 (2021)
30. D. Barrionuevo, N. Ortega, A. Kumar, R. Chatterjee, J.F. Scott, R.S. Katiyar, J. Appl. Phys. **114**, 234103 (2013)
31. Z. Chai, G. Tan, Z. Yue, W. Yang, M. Guo, H. Ren, A. Xia, M. Xue, Y. Liu, L. Lv, Y. Liu, J. Alloys Compd. **746**, 677 (2018)
32. D. Chen, S. Huang, J. Chen, J. Cheng, J. Sol-Gel Sci. Technol. **76**, 220 (2015)

33. S. Yang, F. Zhang, X. Xie, H. Sun, L. Zhang, S. Fan, J. Alloys Compd. **734**, 243 (2018)
34. M. Guo, G. Tan, W. Yang, Y. Liu, H. Ren, A. Xia, L. Lv, M. Xue, Ceram. Int. **44**, 12282 (2018)
35. W. Sun, Z. Zhou, K. Wang, J. Li, J. Appl. Phys. **121**, 064101 (2017)
36. D. Kuang, P. Tang, S. Yang, Y. Zhang, J. Sol-Gel Sci. Technol. **73**, 410 (2015)

Publisher's Note Springer Nature remains neutral with regard to jurisdictional claims in published maps and institutional affiliations.